PHYSICAL REVIEW C **95**, 034303 (2017)

Hybrid configuration mixing model for odd nuclei

G. Colò,* P. F. Bortignon, and G. Bocchi
Dipartimento di Fisica, Università degli Studi di Milano, via Celoria 16, 20133 Milano, Italy
and INFN sezione di Milano, via Celoria 16, 20133, Milano, Italy
(Received 23 December 2016; published 6 March 2017)

In this work, we introduce a new approach which is meant to be a first step towards complete self-consistent low-lying spectroscopy of odd nuclei. So far, we essentially limit ourselves to the description of a double-magic core plus an extra nucleon. The model does not contain any free adjustable parameter and is instead based on a Hartree-Fock (HF) description of the particle states in the core, together with self-consistent random-phase approximation (RPA) calculations for the core excitations. We include both collective and noncollective excitations, with proper care of the corrections due to the overlap between them (i.e., due to the nonorthonormality of the basis). As a consequence, with respect to traditional particle-vibration coupling calculations in which one can only address single-nucleon states and particle-vibration multiplets, we can also describe states of shell-model types like 2 particle–1 hole. We will report results for ^{49}Ca and ^{133}Sb and discuss future perspectives.

DOI: 10.1103/PhysRevC.95.034303

I. INTRODUCTION

Finding a successful microscopic description for the low-lying spectra of odd nuclei is, to a large extent, an open question. A few of them can be reasonably described in terms of an even-even core plus an extra particle, as is well known from the early days of the introduction of the shell model in nuclear physics; at the same time, state-of-the-art applications of self-consistent mean field (SCMF) or density functional theory (DFT) often fail in reproducing the ordering of low-lying levels in the odd system (see, e.g., Ref. [1] and references therein). The detailed spectroscopy of odd nuclei can also be studied within theories that go beyond the simple one-quasiparticle picture. The generator coordinate method (GCM) and multireference DFT (MR-DFT), which include the mixing of various DFT configurations and hence the restoration of broken symmetries, have recently been applied to odd nuclei [2]: At present, these calculations are still very demanding from the computational point of view and thus have limited applicability. Large-scale shell-model calculations are certainly appropriate for spectroscopy and their success in light nuclei is well documented [3]. Nonetheless, they become increasingly difficult when the mass number increases. In our paper, this will become evident as we will mention shell-model calculations around ^{48}Ca and point out that the same calculations are not feasible around ^{132}Sn or for even larger nuclei.

All this points clearly to the need for complementary theoretical approaches that can be transferable among different mass regions and provide sound and transparent results. Particle-vibration coupling (PVC) models are based on the simple yet effective idea that particles (or quasiparticles) outside a spherical core are mainly affected by the low-lying core excitations, so that a proper description of the odd nucleus should result from the treatment of the coupling between particles and core vibrations. This picture has been introduced quite early in nuclear structure theory, both by the Copenhagen [4] and Dubna [5] schools. Most applications have been purely phenomenological (see Ref. [6] for a recent example). In our work, we start instead from a microscopic Hamiltonian of the Skyrme type. There is continuous interest in models based on the interplay between fermionic and bosonic degrees of freedom in nuclei: A novel method has been recently introduced in Ref. [7].

Some of us have already studied single-particle states around a magic core by using PVC based on the Skyrme Hamiltonian [8–10], while similar calculations in the relativistic mean field (RMF) framework have been carried out in Refs. [11,12]. However, the low-lying spectra of odd nuclei are characterized by the simultaneous presence of states having quite different physical nature. The aim of our work is making steps towards complete spectroscopy, rather than focusing only on states with a specific character, as we explain below.

Some of the states in the odd system have indeed mainly particle-like character and accordingly possess large spectroscopic factors associated with stripping and pickup reactions.[1] Some other states may instead have the largest component which is associated with the coupling of a particle with a core vibration. We take as a signature of such character the fact that the reduced decay transition probability from these states to the odd nucleus ground state is similar to the reduced transition probability of the core vibration. In fact, in the weak coupling scheme these reduced transition probabilities are equal, that is,

$$B(E\lambda,[j' \otimes J = \lambda]_j \rightarrow j') = B(E\lambda, J = \lambda \rightarrow 0), \quad (1)$$

where j' and J label, schematically, the particle state and the core vibration coupled to angular momentum j (cf. Eqs. (6.467) and (6.86) of Ref. [4]). Moreover, there might be

*gianluca.colo@mi.infn.it

[1]We are well aware of the problems connected with a clean definition of spectroscopic factors. However, such problems do not prevent use of spectroscopic factors for a qualitative indication about the nature of observed states discussed here.

further states that have, for instance, 2p-1h (or 3p-2h) character and do not fit the PVC scheme by definition. These states appear, naturally, in shell-model calculations.

All these considerations have motivated the formulation of a hybrid model that we shall call the hybrid configuration mixing (HCM) model in what follows. In this model, we include particle states together with states that for practical reasons emerge from random phase approximation (RPA) calculations, but can have either collective character or pure particle-hole (p-h) nature. In either case, we should of course account at our best for Pauli principle violations, the problem being certainly more severe in the case of pure p-h states.

In practice, in this first work devoted to the basics of the model and the first applications, we consider a magic core and one active particle outside it, together with the core excitations having either natural or non-natural parity. The particle states will have the usual quantum numbers n,l,j,m but we shall often use jm in what follows for the sake of simplicity. For each spin and parity $J^\pi M$ the core excitations will be labeled by an index N and we shall often simply write NJM, by dropping the parity label. As explained above, in the model space for the description of the $A+1$ nucleus (where A is even) we include single-particle states j together with coupled states $[j' \otimes J]_j$. We stress again that some of the latter states are genuine particle plus phonon states while others have 2p-1h or mixed character. In this respect, our model is not a simple PVC implementation. We diagonalize in the given model space the Hamiltonian, which includes the mean-field solutions of the Skyrme Hamiltonian (particles and RPA solutions) plus the residual interaction acting among them. Extensions to nonmagic systems, in which pairing should be added and the model is based on quasiparticles and QRPA states, can be envisaged in future.

The details of the model will be elucidated in Sec. II. Section II A deals with the calculation of the energy spectrum, while the determination of the electromagnetic transition probabilities is described in Sec. II B. The detailed formulas for the overlap matrix and for the reduced transition probability are actually derived in the two appendixes. Section III is devoted to a discussion of our results for ^{49}Ca and ^{133}Sb. Conclusions and perspectives are drawn in Sec. IV.

II. THEORETICAL FORMALISM

A. Calculation of the energy spectrum

In our model we solve the Hamiltonian

$$\begin{aligned} H &= H_0 + V, \\ H_0 &= \sum_{jm} \varepsilon_j a^\dagger_{jm} a_{jm} + \sum_{NJM} \hbar\omega_{NJ} \Gamma^\dagger_{NJM} \Gamma_{NJM}, \\ V &= \sum_{jmj'm'} \sum_{NJM} h(jm; j'm', NJM) a_{jm} [a^\dagger_{j'} \otimes \Gamma^\dagger_{NJ}]_{jm}, \end{aligned} \tag{2}$$

where part of the notation has been already introduced. a and $a^\dagger$ are the usual fermion annihilation and creation operators, while the notations Γ and $\Gamma^\dagger$ are used for boson operators. ε and $\hbar\omega$ are, respectively, the energies of single particles and of RPA solutions. The coupling matrix elements h have been already defined in Eq. (A1) of Ref. [8]. Our calculation is self-consistent in the sense that all basis states come out of HF and RPA calculations [13] performed with a Skyrme force, together with the coupling matrix elements. In this sense, there are no free parameters to adjust.

This Hamiltonian can be diagonalized separately in different Hilbert subspaces with good quantum numbers. The basis states in these subspaces have been discussed in the introduction. More precisely, there are either

$$|jm\rangle = a^\dagger_{jm}|0\rangle, \tag{3}$$

where $|0\rangle$ is the even-even core, or

$$\begin{aligned} |[j' \otimes NJ]_{jm}\rangle = \Bigg\{ &\sum_{ph} \sum_{m'Mm_pm_h} \langle j'm'JM|jm\rangle X^{(NJ)}_{ph} (-1)^{j_h - m_h} \langle j_p m_p j_h - m_h | JM\rangle a^\dagger_{j'm'} a^\dagger_{j_p m_p} a_{j_h m_h} |0\rangle \\ &- \sum_{ph} \sum_{m'Mm_pm_h} \langle j'm'JM|jm\rangle Y^{(NJ)}_{ph} (-1)^{j_h - m_h + J + M} \langle j_p m_p j_h - m_h | J - M\rangle a^\dagger_{j'm'} a^\dagger_{j_h m_h} a_{j_p m_p} |0\rangle \Bigg\}, \end{aligned} \tag{4}$$

that are particles coupled to a RPA solution.

The matrix elements h between configurations (3) and (4) are written as $\langle j||V||j'J\rangle/\hat{j}$ (cf. Eq. (A9) of Ref. [8]). Thus, the Hamiltonian in each of the subspaces has the typical form

$$H = \begin{pmatrix} \varepsilon_{n_1 lj} & 0 & \frac{\langle n_1 lj||V||n'_1 l'_1 j'_1 N_1 J_1\rangle}{\hat{j}} & \frac{\langle n_1 lj||V||n'_2 l'_2 j'_2 N_2 J_2\rangle}{\hat{j}} \\ 0 & \varepsilon_{n_2 lj} & \frac{\langle n_2 lj||V||n'_1 l'_1 j'_1 N_1 J_1\rangle}{\hat{j}} & \frac{\langle n_2 lj||V||n'_2 l'_2 j'_2 N_2 J_2\rangle}{\hat{j}} \\ \frac{\langle n_1 lj||V||n'_1 l' j'_1 N_1 J_1\rangle}{\hat{j}} & \frac{\langle n_2 lj||V||n'_1 l' j'_1 N_1 J_1\rangle}{\hat{j}} & \varepsilon_{n'_1 l'_1 j'_1} + \hbar\omega_{N_1 J_1} & 0 \\ \frac{\langle n_1 lj||V||n'_2 j'_2 N_2 J_2\rangle}{\hat{j}} & \frac{\langle n_2 lj||V||n'_2 l' j'_2 N_2 J_2\rangle}{\hat{j}} & 0 & \varepsilon_{n'_2 l'_2 j'_2} + \hbar\omega_{N_2 J_2} \end{pmatrix}. \tag{5}$$

We can label the basis states [either of the type (3) or (4)] with $|i\rangle$, so that the above matrix is $H_{ii'}$. The corresponding eigenvalue equation is then

$$H|\alpha\rangle = E_\alpha|\alpha\rangle, \quad |\alpha\rangle = \sum_i \xi_i^{(\alpha)}|i\rangle. \tag{6}$$

The main issue when solving this equation is that the basis in second subspace [the one spanned by the states (4)] is in general nonorthogonal and overcomplete.

We overcome this problem by using the technique of Ref. [14]. For this aim, we need the overlap matrix between the basis states in the Hilbert subspace under study. The matrix of the overlaps is clearly diagonal in the subspace of states (3), and zero if matrix elements between states of the type (3) and (4) are considered. On the other hand, we do have nontrivial overlaps between states of the type (4). We calculate them by assuming TDA and label them as n. This calculation is carried out in Appendix A. Then, the overlap matrix $\mathcal{N}$ is

$$\mathcal{N} = \begin{pmatrix} 1 & 0 & \dots & 0 & 0 & \dots \\ 0 & 1 & \dots & 0 & 0 & \dots \\ \dots & \dots & \dots & \dots & \dots & \dots \\ 0 & 0 & \dots & n(j_1' n_1 J_1, j_1' n_1 J_1) & n(j_1' n_1 J_1, j_2' n_2 J_2) & \dots \\ 0 & 0 & \dots & n(j_2' n_2 J_2, j_1' n_1 J_1) & n(j_2' n_2 J_2, j_1' n_1 J_1) & \dots \\ \dots & \dots & \dots & \dots & \dots & \dots \end{pmatrix}. \tag{7}$$

Having defined the matrices H and $\mathcal{N}$ we can now follow the steps of Ref. [14]:

(1) We diagonalize the overlap matrix $\mathcal{N}$ so that it assumes a diagonal form Λ with eigenvalues λ_β. The unitary transformation that is associated with this transformation is written as S, so that

$$\Lambda = S^\dagger \mathcal{N} S, \tag{8}$$

with $S^\dagger S = 1$ (cf. p. 1775 of Ref. [14]).

(2) If some eigenvalue λ_β is zero or negative it means that the basis is overcomplete and the corresponding eigenvector $|\beta\rangle$ must be eliminated.

(3) We then solve Eq. (19) of Ref. [14], that is,

$$\mathcal{H}\mathcal{X} = E\mathcal{X}, \tag{9}$$

$$\mathcal{H} = \Lambda^{-1/2} S^\dagger H S \Lambda^{-1/2}, \tag{10}$$

in the reduced space.

(4) The solution provides the physical energies of the system, that is, the eigenvalues E_α.

(5) The eigenvectors can be expressed in terms of the original basis by inverting Eq. (20) of Ref. [14], namely if α is an element of it:

$$X_\alpha = \sum_\beta S_{\alpha\beta} \lambda_\beta^{-1/2} \mathcal{X}_\beta. \tag{11}$$

This procedure provides the result for the excitation energy spectrum. We now turn our attention to the transitions between these states.

B. Electromagnetic transition probabilities

We define the reduced transition probabilities in the standard way as

$$B(X\lambda) \equiv \frac{1}{2j_f+1} |\langle \alpha_f j_f || \hat{O}(X\lambda) || \alpha_i j_i \rangle|^2, \tag{12}$$

where the label X can be either E or M. The reduced matrix element becomes

$$\begin{aligned} &\langle \alpha_f j_f || \hat{O}(X\lambda) || \alpha_i j_i \rangle \\ &= \sum_{if} \xi_i^{\alpha_i} \xi_f^{\alpha_f} \langle f j_f || \hat{O}(X\lambda) || i j_i \rangle \\ &= \sum_{if} \xi_i^{\alpha_i} \xi_f^{\alpha_f} \langle j_f || \hat{O}(X\lambda) || j_i \rangle \\ &\quad + \sum_{if} \xi_i^{\alpha_i} \xi_f^{\alpha_f} \langle [j_f' \otimes J_f']_{j_f} || \hat{O}(X\lambda) || j_i \rangle \\ &\quad + \sum_{if} \xi_i^{\alpha_i} \xi_f^{\alpha_f} \langle j_f || \hat{O}(X\lambda) || [j_i' \otimes J_i]_{j_i} \rangle \\ &\quad + \sum_{if} \xi_i^{\alpha_i} \xi_f^{\alpha_f} \langle [j_f' \otimes J_f']_{j_f} || \hat{O}(X\lambda) || [j_i' \otimes J_i']_{j_i} \rangle, \end{aligned} \tag{13}$$

where we have schematically separated the sum over i, f into four terms, namely the case in which both indices correspond to states (3), the case in which the first index is associated to a state (3) and the second index is associated to a state (4), the case in which i and f are interchanged with respect to the previous case, and finally the case in which both indices correspond to states of the type (4). The electromagnetic operator is the sum of a part acting on single-particle states, $\hat{O}_{\rm sp}$, and a part acting on phonons, $\hat{O}_{\rm ph}$ (for simplicity we drop the label $X\lambda$ in what follows).

We treat separately the four matrix elements appearing in the last four lines of Eq. (13). Their detailed calculation is discussed in Appendix B. By using them, Eq. (13) becomes

$$
\begin{aligned}
&\langle \alpha_f j_f || \hat{O}(X\lambda) || \alpha_i j_i \rangle \\
&= \sum_{if} \xi_i^{\alpha_i} \xi_f^{\alpha_f} \langle j_f || \hat{O}(X\lambda) || j_i \rangle + \sum_{if} \xi_i^{\alpha_i} \xi_f^{\alpha_f} \delta(J'_f,\lambda)\delta(j'_f,j_i) \frac{\hat{j}_f}{\hat{\lambda}} \langle J'_f || \hat{O}_{\rm ph} || 0 \rangle \\
&+ \sum_{if} \xi_i^{\alpha_i} \xi_f^{\alpha_f} \delta(J'_i,\lambda)\delta(j'_i,j_f) \frac{\hat{j}_i}{\hat{\lambda}} \langle J'_i || \hat{O}_{\rm ph} || 0 \rangle (-)^{j_i - j_f + \lambda + \binom{+1 \text{ for M}}{+0 \text{ for E}}} + \sum_{if} \xi_i^{\alpha_i} \xi_f^{\alpha_f} \hat{j}_f \hat{j}_i \left\{ (-)^{j_f + J'_i + \lambda + j'_i} \begin{Bmatrix} j_i & j_f & \lambda \\ J'_f & J'_i & j'_f \end{Bmatrix} \delta(j'_f, j'_i) \right. \\
&\times \sum_{ph,p'h'} \left[X^f_{ph} X^i_{p'h'} + (-)^{J'_f - J'_i + \lambda} Y^f_{ph} Y^i_{p'h'} \right] \left(\delta(h,h') \hat{J}'_f \hat{J}'_i (-)^{j_h + j_p + J'_i + \lambda} \begin{Bmatrix} j_h & J'_i & j_{p'} \\ \lambda & j_p & J'_f \end{Bmatrix} \langle j_p || \hat{O}_{sp} || j_{p'} \rangle \right. \\
&\left. \left. - \delta(p,p') \hat{J}'_f \hat{J}'_i (-)^{j_h + j_p + J'_f} \begin{Bmatrix} j_p & J'_i & j_{h'} \\ \lambda & j_h & J'_f \end{Bmatrix} \langle j_{h'} || \hat{O}_{sp} || j_h \rangle \right) + (-)^{j_i + j'_f + \lambda + J'_f} \begin{Bmatrix} j_f & j_i & \lambda \\ j'_i & j'_f & J'_f \end{Bmatrix} \delta(J'_f, J'_i) \langle j'_f || \hat{O}_{sp} || j'_i \rangle \right\}. \quad (14)
\end{aligned}
$$

III. RESULTS

We will discuss results obtained for ^{49}Ca and ^{133}Sb, namely ^{48}Ca plus one neutron and ^{132}Sn plus one proton. In all cases, we use accordingly the HF and RPA states of the core nucleus. The calculations are based on the use of two Skyrme interactions, namely SkX [15] and SLy5 [16]. We do not want to explore all possible choices of a Skyrme set. These two may be considered quite representative for the following reasons. While the latter is a standard Skrme force with effective mass m^* around $0.7m$, so that it has been built without special attention to the single-particle shell structure around the Fermi energy, the former has been built by including in the fit protocol the single-particle energies of a few magic nuclei (as far as they are experimentally known), including ^{48}Ca and ^{132}Sn.

We first provide some numerical details. The HF equations are solved in coordinate space by using a radial mesh that extends up to 15 fm in the case of ^{48}Ca and 20 fm in the case of ^{132}Sn. The mesh size is 0.1 fm. Then, the RPA basis is built by considering all occupied states and unoccupied states that span 8 values of the radial quantum number n for each value of l and j. This space is large enough so that the appropriate sum rules are fulfilled and the properties of the low-lying states have converged [13].

Finally, a few HF states (typically, the valence shell) and phonon states (up to about 5- or 6-MeV excitation energy) are selected to make up the model space in which the equations that have been laid down in the previous section are solved.

A. ^{49}Ca

For this nucleus, few unoccupied states of ^{48}Ca are selected, namely the neutron orbitals $2p_{3/2}$, $2p_{1/2}$, $1f_{5/2}$, and $1g_{9/2}$. The lowest three are displayed in the first column (from left) of both panels of Fig. 1. The left (right) panel displays the results obtained with the interaction SkX (SLy5). In both cases, the level $1g_{9/2}$ lies above the scale of the figure, that is, more than 5.5 MeV above the ground state of ^{49}Ca. The core excitations obtained by means of the self-consistent RPA are shown in the second column of Fig. 1. We have in fact considered the states having angular momentum between $J = 0$ and 8, either with positive or negative parity, and selected those below 5.5 MeV.

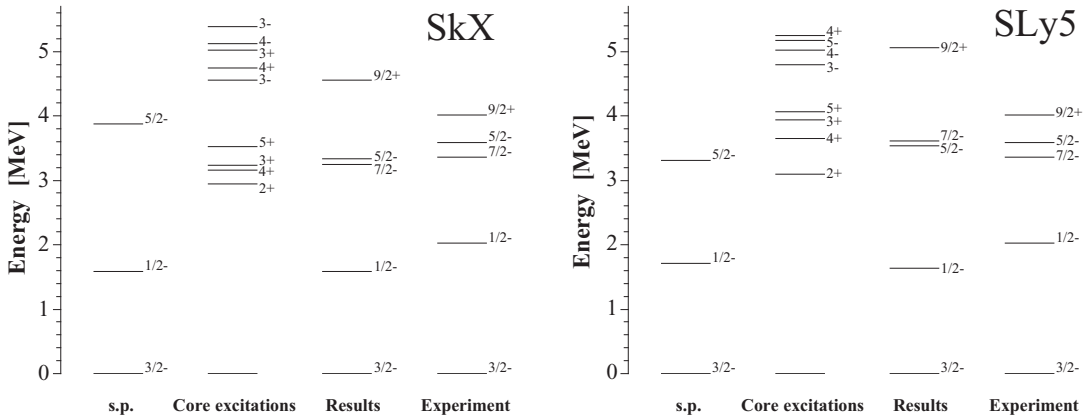

FIG. 1. Low-lying levels of ^{49}Ca. In both panels, in the first column at right the lowest unoccupied single-particle states of the ^{48}Ca are displayed, while the lowest multipole excitations of the same core (below 5.5 MeV) are shown in the second column. The result of the diagonalization described in Sec. II, that is, the lowest states of ^{49}Ca obtained within our model, are presented in the third column and compared with the experimental data in the fourth and last column. The panel at left (right) corresponds to results obtained with the force SkX (SLy5).

TABLE I. Experimental and RPA multipole states of ^{48}Ca. Theoretical prediction for the $B(E/M)$ values refer to the transitions to the ground state. All the theoretical calculation are performed with the two SkX and SLy5 interactions.

J^π	Energy [MeV]			$B(E/M\lambda)$ [W.u.]		
	Exp.	Theory (SkX)	Theory (SLy5)	Exp.	Theory (SkX)	Theory (SLy5)
2_1^+	3.83	2.87	3.02	1.71	1.31	1.12
4_1^+	4.50	3.12	3.60		0.43	0.70
3_1^-	4.51	4.43	4.75	5.0	6.77	6.12
3_1^+	4.61	3.22	3.92		6.6×10^{-4}	6.6×10^{-3}
4_1^-	5.26	5.11	5.01		0.07	1.80
3_2^-	5.37	5.37			0.05	
3_2^+		5.02			7.6×10^{-4}	
4_2^+		4.70	5.20		1.02	0.86
5_1^+		3.51	3.90		5.0×10^{-3}	0.01

There is a clear similarity, but not a close identity, between the results obtained with the two Skyrme sets. In order to let the reader judge about the quality of our reproduction of the experimentally known properties of the core excitations, we display their energies and transition probabilities in Table I.

The results of our calculations are in the third column and can be directly compared with the experimental states of the fourth column. All excitation energies are with respect to the $3/2^-$ ground state of ^{49}Ca, which is set at zero energy. Note that we have chosen to display, besides the ground state, the lowest states of each multipolarity that appear between 0 and 5 MeV, provided an experimentally known state is found and its spin and parity are identified without ambiguities.

The $3/2^-$ ground state has, as expected, mainly a particle character. The overlap between this state and the unperturbed $2p_{3/2}$ is 93% for SkX and 92% for SLy5. A similar statement can be made for the lowest $1/2^-$ state. In this case, the overlap with the unperturbed $2p_{1/2}$ is about 85% for SkX and 87% for SLy5. The energies of the $1/2^-$ state and those of the pure $2p_{1/2}$ state are quite similar for both Skyrme sets. On the other hand, the $5/2^-$ state is practically a pure $1p_{3/2}$ coupled to the 2^+ phonon of ^{48}Ca in the case of SkX, but in the case of SLy5 such component decreases to 51% and the state has admixtures of single-particle $1f_{5/2}$ (plus other smaller components). From the figure, one understands this is related to the smaller energy difference between the 2^+ phonon and the $1f_{5/2}$ state in the case of SLy5. The state $7/2^-$ is to a large extent, in our model, a member of the $1p_{3/2} \otimes 2_1^+$ multiplet for both Skyrme forces and is very close to the $5/2^-$ (although one can note a level inversion in the case of SLy5). Finally, the $9/2^+$ state has a large percentage in its wave function, of about 87% for SkX and 90% with SLy5, associated with the $1p_{3/2} \otimes 3_1^-$ component (where 3_1^- is the lowest collective octupole phonon of the core).

In summary, the model is able to predict states of different characters that reproduce the sequence that is experimentally observed. In almost all the cases, the results do not depend significantly on the chosen Skyrme set except when some case of quasidegeneracy creates some difference. The theoretical spectrum is somehow more stretched than the experimental one, in a more pronounced manner for SLy5 than for SkX. The rms difference between experimental and theoretical energies is 0.429 MeV for SkX and 0.661 MeV for SLy5: We stress again that we do not adjust any parameter to obtain these results. We now turn to the analysis of the electromagnetic transitions.

The transition from the $9/2^+$ excited state to the $3/2^-$ ground state has been evidenced and discussed in Ref. [17]. In that work, some of us have used the lowest order perturbative estimate for the $E3$ transition, based on the weak-coupling model of Ref. [4] and accordingly on the above Eq. (1). The $9/2^+$ is taken in this case as a member of the $2p_{3/2} \otimes 3_1^-$ multiplet. Within that framework, the $E3$ decay transition probability is equal to that of the 3_1^- lowest phonon of ^{48}Ca, which was reported to be 7.0 W.u. [17,18] if the interaction SLy5 [16] is used.

We have come back to this analysis in the present work. Within the framework of the fully microscopic, nonperturbative model, at variance with the assumption of the weak coupling model, the overlap between the ground state (g.s.) and the pure $2p_{3/2}$ particle state is 93% as already said and the overlap between the $9/2^+$ state and the pure $2p_{3/2} \otimes 3_1^-$ state is also smaller than 100%. Due to this, and to the presence of other small components in the wave functions, we obtain the results for the $E3$ transition probability that are reported in Table II, namely 5.7 W.u. in the case of SLy5 and 6.4 W.u. in the case of SkX. The latter is in full agreement with the experimental value, while the former is slightly underestimated.

In the table, we also show the result for the $E2$ transition between the states $7/2^-$ and $3/2^-$. In our model, the $7/2^-$ state is essentially a pure $2p_{3/2} \otimes 2_1^+$ state. Thus, we obtain a value of the $B(E2)$ which is close to the $B(E2)$ of the lowest 2_1^+ phonon of the core, that is, 1.3 W.u. in the case of SkX and 1.1 W.u. in the case of SLy5: These values compare rather well with the experimental one of 1.7 W.u. Experiment seems to indicate some more mixing with other components than the simple $2p_{3/2} \otimes 2_1^+$ state.

The analysis of the electromagnetic transitions confirms that there are quantitative but not qualitative differences between the results obtained with the two different Skyrme sets. We shall display results obtained with SkX in what follows.

B. ^{133}Sb

Concerning the ^{133}Sb nucleus, few unoccupied states of ^{132}Sn are selected, namely the proton orbitals $1g_{7/2}$, $2d_{5/2}$,

TABLE II. Reduced electromagnetic transition probabilities that have been experimentally measured for ^{49}Ca in Ref. [17], compared with the result from the present model.

	Theory		Exp.
	SkX	SLy5	
$B(E3, 9/2^+ \to 3/2^-)$	6.4	5.7	7.9 ± 2.0 W.u.
$B(E2, 7/2^- \to 3/2^-)$	1.4	1.0	0.05 ± 0.02 W.u.

$2d_{3/2}$, $1h_{11/2}$, and $3s_{1/2}$. These five single particle states are displayed in the first column (from left) of Fig. 2. As in the previous case, the core excitations are obtained by means of the self-consistent RPA and they are shown in the second column of Fig. 2. We have in fact considered the states having angular momentum between $J = 0$ and $J = 12$, either with positive and negative parity, and selected those below 5.5 MeV. We show the properties of these states in Table III. We do not simply show the energies and transition probabilities, but also the main components of the wave function as they emerge from the RPA calculation. The collective or noncollective nature of these excitations is quite evident.

The results of our calculations are in the third column of Fig. 2 and can be directly compared with the experimental states of the fourth column. All excitation energies are with respect to the $7/2^+$ ground state of ^{133}Sb which is set at zero energy. Note that we have chosen to display, besides the ground state, the lowest states of each multipolarity that appear between 0 and 5 MeV, provided an experimentally known state is found and its spin and parity are identified without ambiguities. We now discuss the theoretical results.

The $7/2^+$ ground state has, as expected, mainly a single-particle character. The overlap between this state and the unperturbed $1g_{7/2}$ is 97%. A similar statement can be made for the lowest three excited states below 3 MeV, the $5/2^+$, $3/2^+$, and $11/2^-$ states. In this case, the overlap with the unperturbed $2d_{5/2}$, $2d_{3/2}$, and $1h_{11/2}$ are, respectively, about 94%, 83%, and 92%. The energies of these states are accordingly quite similar to those of the single-particle states calculated with SkX.

The scenario starts to change considering the $11/2^+$ state. In this case, the wave function has a quite large percentage, of about 77%, associated with the $1g_{7/2} \otimes 2_1^+$ (where 2_1^+ is the lowest collective quadrupole phonon of the core) component. A non-negligible part of the wave function is composed by 2p-1h states, mainly the $\pi 1g_{7/2} \nu h_{11/2}^{-1} f_{7/2}$. In our representation, these components manifest themselves as $1g_{7/2} \otimes 3_1^+$ and $1g_{7/2} \otimes 8_1^+$. An evolution in the wave function composition can be observed with increasing spin; indeed the $13/2^+$ and the $15/2^+$ states show a fragmented wave function involving the coupling of the valence proton $1g_{7/2}$ to both the 4_1^+ phonon (33%) and noncollective p-h excitations. Finally, the highest spin states $17/2^+$ and the $21/2^+$ are dominated by the valence proton coupled to the neutron $h_{11/2}^{-1} f_{7/2}$ noncollective core excitation (67% and 92% respectively).

In summary, the model provides a very good overall description of this spectrum in which states of different nature coexist. As in ^{49}Ca, the theoretical spectrum is somehow more stretched than the experimental one. The negative-parity

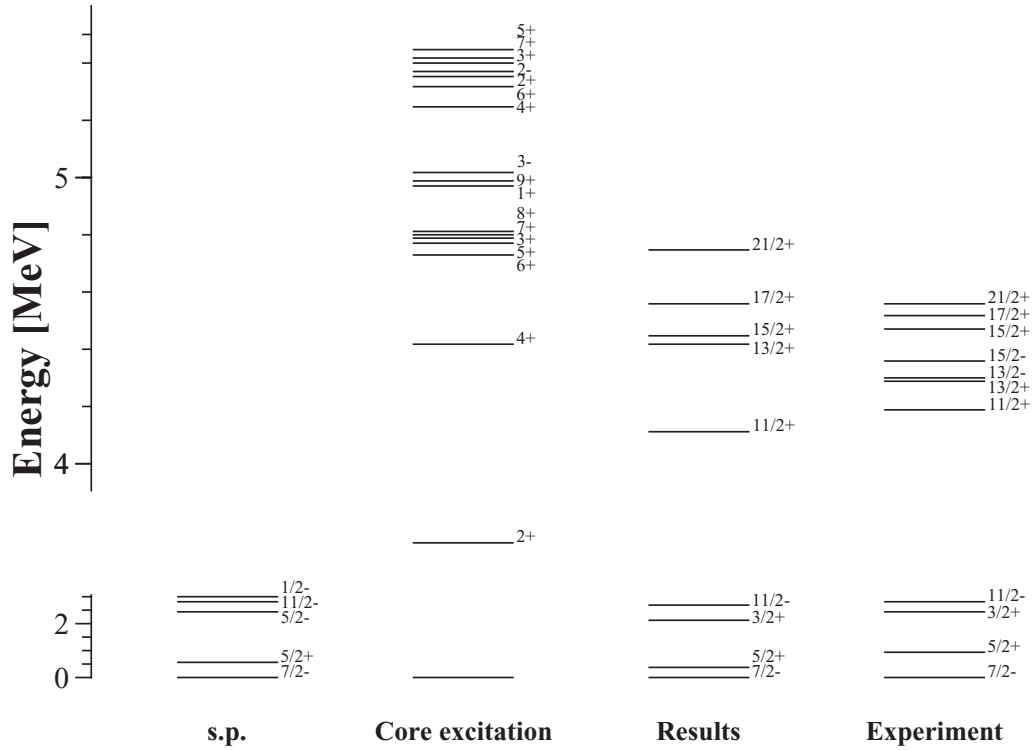

FIG. 2. The same as Fig. 1 for the case of ^{133}Sb, except that here only the results corresponding to the force SkX are shown.

TABLE III. Experimental and RPA multipole states of ^{132}Sn. The main components are those associated with RPA amplitudes X that are larger than 0.3 in absolute value, and are listed together with the value of X^2 in parentheses.

J^π	Energy [MeV]		$B(E/M\lambda)$ [W.u.]		Main components
	Exp.	Theory	Exp.	Theory	Theory
2_1^+	4.041	3.87	7	4.75	$\nu h_{11/2}^{-1} f_{7/2}$ (0.56), $\pi g_{9/2}^{-1} d_{5/2}$ (0.19), $\pi g_{9/2}^{-1} g_{7/2}$ (0.14)
3_1^-	4.352	5.02	>7.1	9.91	$\nu s_{1/2}^{-1} f_{7/2}$ (0.40), $\nu d_{3/2}^{-1} f_{7/2}$ (0.12), $\pi p_{1/2}^{-1} g_{7/2}$ (0.12)
4_1^+	4.416	4.42	4.42	5.10	$\nu h_{11/2}^{-1} f_{7/2}$ (0.63), $\pi g_{9/2}^{-1} g_{7/2}$ (0.21)
6_1^+	4.716	4.73		1.65	$\nu h_{11/2}^{-1} f_{7/2}$ (0.86), $\pi g_{9/2}^{-1} g_{7/2}$ (0.11)
8_1^+	4.848	4.80		0.28	$\nu h_{11/2}^{-1} f_{7/2}$ (0.98)
5_1^+	4.885	4.77		0.20	$\nu h_{11/2}^{-1} f_{7/2}$ (0.99)
7_1^+	4.942	4.80		0.30	$\nu h_{11/2}^{-1} f_{7/2}$ (0.98)
(9_1^+)	5.280	4.99		0.04	$\nu h_{11/2}^{-1} f_{7/2}$ (0.99)
1_1^+		4.97		7.95	$\pi g_{9/2}^{-1} g_{7/2}$ (0.76), $\nu h_{11/2}^{-1} h_{9/2}$ (0.24)
2_2^+		5.37		$<10^{-2}$	$\pi g_{9/2}^{-1} g_{7/2}$ (0.72), $\nu h_{11/2}^{-1} f_{7/2}$ (0.18)
2_1^-		5.44		0.47	$\nu d_{3/2}^{-1} f_{7/2}$ (0.79)
3_1^+		4.79		0.13	$\nu h_{11/2}^{-1} f_{7/2}$ (0.96)
3_2^+		5.40		1.99	$\pi g_{9/2}^{-1} g_{7/2}$ (0.96)
4_2^+		5.25		1.01	$\pi g_{9/2}^{-1} d_{3/2}$ (0.56), $\nu h_{11/2}^{-1} f_{7/2}$ (0.32)
5_2^+		5.45		0.61	$\pi g_{9/2}^{-1} g_{7/2}$ (0.99)
6_2^+		5.32		2.67	$\pi g_{9/2}^{-1} g_{7/2}$ (0.74), $\nu h_{11/2}^{-1} f_{7/2}$ (0.13)
7_2^+		5.42		0.50	$\pi g_{9/2}^{-1} g_{7/2}$ (0.99)

states $13/2^-$ and $15/2^-$ constitute the only exceptions to the excellent performance of our model in reproducing the experimental energies. In fact, the rms deviation between experimental and theoretical energies is 0.869 MeV but drops dramatically to 0.246 MeV if these two states are excluded. This latter number is in harmony with the result from ^{49}Ca, if one takes into account the overall scaling of the energy of the nuclear levels that goes like $A^{-1/3}$. The $13/2^-$ state is too high, as it lies at 5.56 MeV while experimentally it is found at 4.2 MeV. It turns out to be completely made up with the $2g_{7/2} \otimes 3_1^-$ configuration and, as a consequence, the fact that the 3^- state in ^{132}Sn is too high with respect to the experimental finding certainly has an impact. At the same time, the inclusion in our model space of higher energy states, and/or of the coupling with other configurations, may also eventually help to push down its energy. The other state which is too high in energy (6.71 MeV whereas the experimental value is 4.36 MeV) is the $15/2^-$ one and one may think in similar terms. Note that these two states are above the scale of the figure.

TABLE IV. Reduced electromagnetic transitions, which are reported in Table IV probabilities that have been recently experimentally measured in Ref. [19] in ^{133}Sb, compared with the results from the present model.

	Theory	Exp.
$B(M1, 15/2^+ \to 13/2^+)$	0.021	>0.24 W.u.
$B(M1, 13/2^+ \to 11/2^+)$	0.001	0.0042 ± 0.0015 W.u.

We now turn to the analysis of the electromagnetic transitions, which are reported in Table IV.

From the experimental point of view, the transition from the $15/2^+$ to the $13/2^+$ state and from the $13/2^+$ to the $11/2^+$ state have been recently measured and discussed in Ref. [19]; in that work, some of us have pointed out a large difference ($\approx$60) between the $B(M1)$ values of the $15/2^+ \to 13/2^+$ and the $13/2^+ \to 11/2^+$ transitions. This large ratio can be understood in a very transparent way within the framework of the current model. Our theory provides the values of 0.021 μ_N^2 and 0.001 μ_N^2, in the case of the $15/2^+ \to 13/2^+$ and $13/2^+ \to 11/2^+$ transition, respectively. In fact, the $15/2^+$ and $13/2^+$ states have a similar wave functions, and its largest component is the 2p-1h configuration $\pi g_{7/2}\, \nu h_{11/2}^{-1} f_{7/2}$, with an amplitude of the order of 0.4. The transition matrix element $\langle 13/2^+ || O(M1) || 11/2^+ \rangle$ would be 4.86 μ_N if a pure $(\pi g_{7/2}\, \nu h_{11/2}^{-1} f_{7/2})$ component were assumed for both states, leading to a $B(M1)$ of 1.69 μ_N^2. Including the product of the two amplitudes of the order of 0.4, we obtain a $B(M1)$ around 0.04 μ_N^2, close to the value of the full calculation. However, if we assumed the same purity for the $11/2^+$ state, the transition matrix element would remain approximately the same. Instead, in our model, the compositions of $13/2^+$ and $11/2^+$ states are very different, leading to a much more quenched value of the $B(M1)$. In particular, the $11/2^+$ state has a significant particle-phonon configuration and thus a poor overlap with the simple $(\pi g_{7/2}\, \nu h_{11/2}^{-1} f_{7/2})$ component. In conclusion, theory provides a ratio of 20 between the two values of the transition probability, which is in qualitative agreement with the experimental value and, more importantly, can be understood from the point of view of this

model. The measurement of such transition probabilities is a unique signature of the nontrivial change of configuration mixing in the $11/2^+$, $13/2^+$, and $15/2^+$ states of the ^{133}Sb nuclues.

IV. CONCLUSIONS

In this work, we have undertaken a first step to generalize the concept of PVC calculations, in a nonperturbative way, for the case of odd nuclei made up with a particle around a magic core. We have coupled single-particle states from HF calculations, not only with genuine vibrations of the core but with all the excitations emerging from RPA calculations that include both collective and noncollective states. The problem is formulated in terms of a generalized eiganvalue problem: A norm matrix is introduced that corrects for the fact that states made up with one particle and one core excitation may not form an orthonormal basis.

We have applied this model to ^{49}Ca and ^{133}Sb. We have compared the energy of the states at low energy, and some electromagnetic transitions, with experimental values. The model in its simplicity can account well for the ordering and the absolute energy of the low-lying states, with discrepncies of the order of few hundreds of keV on the scale of 0–5 MeV. It has to be noted that no parameter is specifically adjusted, and HF states, RPA core excitations, as well as the matrix elements that couple them, come out from the use of a Skyrme interaction like SkX or SLy5.

There are open problems, though. The spectra are more stretched in theory than in the experimental findings. Some states, as has been discussed above, deviate more from experiment than the average. Clearly, the picture should be made more complete and the model must be improved by including both the interaction between the particle plus core excitation states, and the contribution of more complicated configurations. We envisage to consider some specific case, starting from well-known nuclei like ^{209}Bi where PVC calculations have been performed in the past [20,21], and test the model convergence as more configurations and/or more mutual interaction terms are added.

Eventually, the model can be applied to other cases of current interest. The nuclei that have been discussed in this work have been object of quite recent experimental studies aimed at completing the spectroscopic information which was so far quite scarce. They are interesting neutron-rich systems but not weakly bound ones. Our model can be eventually applied to more neutron-rich systems where continuum coupling plays a relevant role, thanks to the possibility of performing RPA calculations. Other interesting cases may be spherical nuclei close to a shape phase transition as our model may shed new light on this phenomenon. In general, we deem that it can provide a transparent picture that complements shell-model or GCM calculations, or it may be of great usefulness in mass regions where such calculations are computationally too demanding.

ACKNOWLEDGMENTS

We would like to thank B. Fornal and S. Leoni for many stimulating discussions on the experimental status and the theoretical interpretation of the existing and of the new spectroscopic information. Funding from the European Union's Horizon 2020 research and innovation programme under Grant agreement No. 654002 is acknowledged.

APPENDIX A: CALCULATION OF NONTRIVIAL OVERLAPS

We want to calculate the nontrivial overlaps between stated defined by Eq. (4):

$$\begin{aligned}\langle [j_1' \otimes n_1 J_1]_{jm} | [j_2' \otimes n_2 J_2]_{jm} \rangle = & \sum_{p_1 h_1 p_2 h_2} \sum_{m_1' M_1 m_{p_1} m_{h_1}} \sum_{m_2' M_2 m_{p_2} m_{h_2}} \langle j_1' m_1' J_1 M_1 | jm \rangle \langle j_2' m_2' J_2 M_2 | jm \rangle X^{(n_1 J_1)}_{p_1 h_1} X^{(n_2 J_2)}_{p_2 h_2} \\ & \times (-)^{j_{h_1} - m_{h_1} + j_{h_2} - m_{h_2}} \langle j_{p_1} m_{p_1} j_{h_1} - m_{h_1} | J_1 M_1 \rangle \langle j_{p_2} m_{p_2} j_{h_2} - m_{h_2} | J_2 M_2 \rangle \\ & \times \langle 0 | a^\dagger_{j_{h_1} m_{h_1}} a_{j_{p_1} m_{p_1}} a_{j_1' m_1'} a^\dagger_{j_2' m_2'} a^\dagger_{j_{p_2} m_{p_2}} a_{j_{h_2} m_{h_2}} | 0 \rangle . \end{aligned} \tag{A1}$$

The latter expectation value is

$$\delta(h_1,h_2)\delta(p_1,p_2)\delta(j_1',j_2')\delta(m_1',m_2') - \delta(h_1,h_2)\delta\left(j_{p_1},j_2'\right)\delta\left(m_{p_1},m_2'\right)\delta\left(j_1',j_{p_2}\right)\delta\left(m_1',m_{p_2}\right),$$

so that the overlap becomes

$$\begin{aligned}&\langle [j_1' \otimes n_1 J_1]_{jm} | [j_2' \otimes n_2 J_2]_{jm} \rangle \\ &= \Bigg[\sum_{p_1 h_1} \sum_{m_1' M_1 m_{p_1} m_{h_1} M_2} \langle j_1' m_1' J_1 M_1 | jm \rangle \langle j_1' m_1' J_2 M_2 | jm \rangle X^{(n_1 J_1)}_{p_1 h_1} X^{(n_2 J_2)}_{p_1 h_1} \left\langle j_{p_1} m_{p_1} j_{h_1} - m_{h_1} \middle| J_1 M_1 \right\rangle \left\langle j_{p_1} m_{p_1} j_{h_1} - m_{h_1} \middle| J_2 M_2 \right\rangle \delta(j_1', j_2') \\ &\quad - \sum_{h_1} \sum_{m_1' M_1 m_{h_1}} \sum_{m_2' M_2} \langle j_1' m_1' J_1 M_1 | jm \rangle \langle j_2' m_2' J_2 M_2 | jm \rangle X^{(n_1 J_1)}_{j_2' h_1} X^{(n_2 J_2)}_{j_1' h_1} \left\langle j_2' m_2' j_{h_1} - m_{h_1} \middle| J_1 M_1 \right\rangle \left\langle j_1' m_1' j_{h_1} - m_{h_1} \middle| J_2 M_2 \right\rangle \Bigg] \end{aligned}$$

$$
\begin{aligned}
&= \Bigg[\sum_{p_1 h_1} \sum_{m'_1 M_1} \delta(J_1,J_2) \langle j'_1 m'_1 J_1 M_1 | j m \rangle \langle j'_1 m'_1 J_1 M_1 | j m \rangle X^{(n_1 J_1)}_{p_1 h_1} X^{(n_2 J_1)}_{p_1 h_1} \delta(j'_1, j'_2) \\
&\quad - \sum_{h_1} \sum_{m'_1 M_1 m_{h_1}} \sum_{m'_2 M_2} \langle j'_1 m'_1 J_1 M_1 | j m \rangle \langle j'_2 m'_2 J_2 M_2 | j m \rangle X^{(n_1 J_1)}_{j'_2 h_1} X^{(n_2 J_2)}_{j'_1 h_1} \left\langle j'_2 m'_2 j_{h_1} m_{h_1} \middle| J_1 M_1 \right\rangle \left\langle j'_1 m'_1 j_{h_1} m_{h_1} \middle| J_2 M_2 \right\rangle \Bigg] \\
&= \sum_{p_1 h_1} X^{(n_1 J_1)}_{p_1 h_1} X^{(n_2 J_1)}_{p_1 h_1} \delta(j'_1, j'_2) \delta(J_1, J_2) - \sum_{h_1} (-)^{J_1 + J_2 + j'_1 + j'_2} \hat{J}_1 \hat{J}_2 \begin{Bmatrix} j'_2 & j_{h_1} & J_1 \\ j'_1 & j & J_2 \end{Bmatrix} X^{(n_1 J_1)}_{j'_2 h_1} X^{(n_2 J_2)}_{j'_1 h_1} \\
&= \delta(j'_1, j'_2) \delta(n_1, n_2) \delta(J_1, J_2) - \sum_{h_1} (-)^{J_1 + J_2 + j'_1 + j'_2} \hat{J}_1 \hat{J}_2 \begin{Bmatrix} j'_2 & j_{h_1} & J_1 \\ j'_1 & j & J_2 \end{Bmatrix} X^{(n_1 J_1)}_{j'_2 h_1} X^{(n_2 J_2)}_{j'_1 h_1} \\
&= \delta(j'_1, j'_2) \delta(n_1, n_2) \delta(J_1, J_2) - \sum_{h_1} (-)^{j + j_{h_1}} \hat{J}_1 \hat{J}_2 \; W(j'_1 J_1 J_2 j'_2; j j_{h_1}) X^{(n_1 J_1)}_{j'_2 h_1} X^{(n_2 J_2)}_{j'_1 h_1}.
\end{aligned} \tag{A2}
$$

This quantity will be called as $n(j'_1 n_1 J_1, j'_2 n_2 J_2)$ in the main text.

Just for the sake of understanding, the second term can be looked at in the case $J_1 = J_2 = 0$. It becomes

$$
\sum_{h_1} (-)^{j'_2 + j_{h_1} + J_1} \frac{1}{\hat{j}^2_{h_1}} \delta(j_{h_1}, j'_1) \delta(j_{h_1}, j'_2) \delta(j_{h_1}, j) X^{(n_1 J_1)}_{j'_2 h_1} X^{(n_2 J_2)}_{j'_1 h_1} = - \sum_{h_1} \frac{1}{\hat{j}^2} X^{(n_1)}_{j h_1} X^{(n_2)}_{j h_1}. \tag{A3}
$$

If we have only one hole state h_1 and one particle state j, with the same degeneracy, we expect only one phonon n and the overlap becomes

$$
n = 1 - \frac{1}{2j+1}, \tag{A4}
$$

which seems quite intuitive as the state cannot have norm one but just one of the $2j+1$ magnetic substates is occupied by a particle.

APPENDIX B: CALCULATION OF THE MATRIX ELEMENTS THAT ENTER THE REDUCED ELECTROMAGNETIC TRANSITION PROBABILITY

We discuss here the four matrix elements appearing in the last four lines of Eq. (13): They correspond to the possible transition amplitudes appearing in the electromagnetic transitions between coupled states made up with a single particle and a core excitation.

The first matrix element of Eq. (13) corresponds to the standard single-particle transitions and can be found in textbooks. The second one is finite only in the case of a phonon transition, and becomes, using Eq. (28) at p. 479 of Ref. [22] and other properties of $9j$ and $6j$ symbols,

$$
\begin{aligned}
\langle [j'_f \otimes J'_f]_{j_f} || \hat{O} || j_i \rangle &= \left\langle [j'_f \otimes J'_f]_{j_f} \middle| \middle| [\hat{1}_{\rm sp} \otimes \hat{O}_{\rm ph}]_\lambda \middle| \middle| [j_i \otimes 0_i]_{j_i} \right\rangle \\
&= \hat{\lambda} \hat{j}_i \hat{j}_f \begin{Bmatrix} 0 & \lambda & \lambda \\ j'_f & J'_f & j_f \\ j_i & 0 & j_i \end{Bmatrix} \hat{j}_i \delta(j'_f, j_i) \langle J'_f || \hat{O}_{\rm ph} || 0 \rangle \\
&= \hat{\lambda} \hat{j}_i^2 \hat{j}_f \frac{(-)^{j_f + \lambda + j_i}}{\hat{\lambda} \hat{j}_i} \begin{Bmatrix} j_i & j_f & \lambda \\ J'_f & 0 & j_i \end{Bmatrix} \delta(j'_f, j_i) \langle J'_f || \hat{O}_{\rm ph} || 0 \rangle \\
&= \hat{j}_i \hat{j}_f (-)^{j_f + \lambda + j_i} \delta(J'_f, \lambda) \frac{(-)^{j_i + J'_f + j_f}}{\hat{j}_i \hat{\lambda}} \delta(j'_f, j_i) \langle J'_f || \hat{O}_{\rm ph} || 0 \rangle \\
&= \frac{\hat{j}_f}{\hat{\lambda}} \delta(j'_f, j_i) \delta(J'_f, \lambda) \langle J'_f || \hat{O}_{\rm ph} || 0 \rangle.
\end{aligned} \tag{B1}
$$

The same formula holds in the case of the matrix element of the third line. We finally work out the matrix element in the fourth line.

$$\begin{aligned}
&\left\langle [j'_f \otimes J'_f]_{j_f} \right| \left| [[\hat{1}_{\rm sp} \otimes \hat{O}_{\rm ph}]_\lambda + [\hat{O}_{\rm sp} \otimes \hat{1}_{\rm ph}]_\lambda \right| \left| [j'_i \otimes J'_i]_{j_i} \right\rangle \\
&= \hat{j}_f \hat{j}_i \hat{\lambda} \left(\begin{Bmatrix} 0 & \lambda & \lambda \\ j'_f & J'_f & j_f \\ j'_i & J'_i & j_i \end{Bmatrix} \delta(j'_f, j'_i) \hat{j}'_f \langle J'_f || \hat{O}_{\rm ph} || J'_i \rangle + \begin{Bmatrix} \lambda & 0 & \lambda \\ j'_f & J'_f & j_f \\ j'_i & J'_i & j_i \end{Bmatrix} \delta(J'_f, J'_i) \hat{J}'_f \langle j'_f || \hat{O}_{\rm sp} || j'_i \rangle \right) \\
&= \hat{j}_f \hat{j}_i \left((-)^{j_f + J'_i + \lambda + j'_i} \begin{Bmatrix} j_i & j_f & \lambda \\ J'_f & J'_i & j'_f \end{Bmatrix} \delta(j'_f, j'_i) \langle J'_f || \hat{O}_{ph} || J'_i \rangle \right. \\
&\left. (-)^{j_i + j'_f + \lambda + J'_f} \begin{Bmatrix} j_f & j_i & \lambda \\ j'_i & j'_f & J'_f \end{Bmatrix} \delta(J'_f, J'_i) \langle j'_f || \hat{O}_{sp} || j'_i \rangle \right).
\end{aligned} \tag{B2}$$

The quantity $\langle J'_f || \hat{O}_{ph} || J'_i \rangle$ can be found, e.g., in Ref. [23] in terms of the RPA amplitudes. From Eq. (11.286), in fact,

$$\langle J'_f || \hat{O}_{ph} || J'_i \rangle = \sum_{ph,p'h'} \left[X^f_{ph} X^i_{p'h'} + (-)^{J'_f - J'_i + \lambda} Y^f_{ph} Y^i_{p'h'} \right] \left\langle [ph^{-1}]_{J'_f} \right| \left| \hat{O}_{ph} \right| \left| [p'h'^{-1}]_{J'_i} \right\rangle. \tag{B3}$$

The latter matrix element is given by

$$\begin{aligned}
\left\langle [ph^{-1}]_{J'_f M'_f} \right| \hat{O}_{ph} \left| [p'h'^{-1}]_{J'_i M'_i} \right\rangle &= \frac{1}{\sqrt{2J'_f + 1}} \langle J'_i M'_i \lambda \mu | J'_f M'_f \rangle \left\langle [ph^{-1}]_{J'_f} \right| \left| \hat{O}_{ph} \right| \left| [p'h'^{-1}]_{J'_i} \right\rangle \\
\left\langle [ph^{-1}]_{J'_f} \right| \left| \hat{O}_{ph} \right| \left| [p'h'^{-1}]_{J'_i} \right\rangle &= \sum_{M'_i M'_f \mu} \frac{1}{\sqrt{2J'_f + 1}} \langle J'_i M'_i \lambda \mu | J'_f M'_f \rangle \left\langle [ph^{-1}]_{J'_f M'_f} \right| \hat{O}_{ph} \left| [p'h'^{-1}]_{J'_i M'_i} \right\rangle \\
&= \sum_{M'_i M'_f \mu} \sum_{m_p m_h m_{p'} m_{h'}} \frac{1}{\sqrt{2J'_f + 1}} (-)^{j_h - m_h + j_{h'} - m_{h'}} \langle J'_i M'_i \lambda \mu | J'_f M'_f \rangle \\
&\quad \times \langle j_p m_p j_h - m_h | J'_f M'_f \rangle \langle j_{p'} m_{p'} j_{h'} - m_{h'} | J'_i M'_i \rangle \langle j_p m_p, j_h m_h | \hat{O}_{ph} | j_{p'} m_{p'}, j_{h'} m_{h'} \rangle.
\end{aligned} \tag{B4}$$

The latter matrix element reads

$$\begin{aligned}
\sum_{\alpha\beta} O_{\alpha\beta} \langle 0 | a^\dagger_h a_p : a^\dagger_\alpha a_\beta : a^\dagger_{p'} a_{h'} | 0 \rangle &= \delta(h,h') O_{pp'} - \delta(p,p') O_{hh'} \\
&= \frac{\delta(h,h')}{\sqrt{2j_p + 1}} \langle j_{p'} m_{p'} \lambda \mu | j_p m_p \rangle \langle j_p || \hat{O} || j_{p'} \rangle - \frac{\delta(p,p')}{\sqrt{2j_{h'} + 1}} \langle j_h m_h \lambda \mu | j_{h'} m_{h'} \rangle \langle j_{h'} || \hat{O} || j_h \rangle .
\end{aligned} \tag{B5}$$

Thus, we obtain

$$\begin{aligned}
\left\langle [ph^{-1}]_{J'_f} \right| \left| \hat{O}_{ph} \right| \left| [p'h'^{-1}]_{J'_i} \right\rangle &= \sum_{M'_i M'_f \mu} \sum_{m_p m_h m_{p'} m_{h'}} \frac{1}{\sqrt{2J'_f + 1}} \langle J'_i M'_i \lambda \mu | J'_f M'_f \rangle \\
&\quad \times \langle j_p m_p j_h - m_h | J'_f M'_f \rangle \langle j_{p'} m_{p'} j_{h'} - m_{h'} | J'_i M'_i \rangle \frac{\delta(h,h')}{\sqrt{2j_p + 1}} \langle j_{p'} m_{p'} \lambda \mu | j_p m_p \rangle \langle j_p || \hat{O} || j_{p'} \rangle \\
&\quad - \sum_{M'_i M'_f \mu} \sum_{m_p m_h m_{p'} m_{h'}} \frac{1}{2J'_f + 1} (-)^{j_h - m_h + j_{h'} - m_{h'}} \langle J'_i M'_i \lambda \mu | J'_f M'_f \rangle \\
&\quad \times \langle j_p m_p j_h - m_h | J'_f M'_f \rangle \langle j_{p'} m_{p'} j_{h'} - m_{h'} | J'_i M'_i \rangle \frac{\delta(p,p')}{\sqrt{2j_{h'} + 1}} \langle j_h m_h \lambda \mu | j_{h'} m_{h'} \rangle \langle j_{h'} || \hat{O} || j_h \rangle \\
&= \delta(h,h') \hat{J}'_f \hat{J}'_i (-)^{j_h + j_p + J' i + \lambda} \begin{Bmatrix} j_h & J'_i & j_{p'} \\ \lambda & j_p & J'_f \end{Bmatrix} \langle j_p || \hat{O} || j_{p'} \rangle \\
&\quad - \delta(p,p') \hat{J}'_f \hat{J}'_i (-)^{j_h + j_p + J'_f} \begin{Bmatrix} j_p & J'_i & j_{h'} \\ \lambda & j_h & J'_f \end{Bmatrix} \langle j_{h'} || \hat{O} || j_h \rangle .
\end{aligned} \tag{B6}$$

[1] N. Schunck, J. Dobaczewski, J. McDonnell, J. Moré, W. Nazarewicz, J. Sarich, and M. V. Stoitsov, Phys. Rev. C **81**, 024316 (2010).
[2] B. Bally, B. Avez, M. Bender, and P.-H. Heenen, Phys. Rev. Lett. **113**, 162501 (2014).
[3] E. Caurier, G. Martínez-Pinedo, F. Nowacki, A. Poves, and A. P. Zuker, Rev. Mod. Phys. **77**, 427 (2005).
[4] A. Bohr and B. M. Mottelson, *Nuclear Structure. Volume II: Nuclear Deformations* (W. A. Benjamin, New York, 1980).
[5] V. G. Soloviev, *Theory of Atomic Nuclei: Quasiparticles and Phonons* (Institute of Physics Publishing, Bristol, PA, 1992).
[6] A. Idini, G. Potel, F. Barranco, E. Vigezzi, and R. A. Broglia, Phys. Rev. C **92**, 031304 (2015).
[7] K. Nomura, T. Niksic, and D. Vretenar, Phys. Rev. C **93**, 054305 (2016).
[8] G. Colò, H. Sagawa, and P. F. Bortignon, Phys. Rev. C **82**, 064307 (2010).
[9] K. Mizuyama, G. Colò, and E. Vigezzi, Phys. Rev. C **86**, 034318 (2012).
[10] L. G. Cao, G. Colo, H. Sagawa, and P. F. Bortignon, Phys. Rev. C **89**, 044314 (2014).
[11] E. Litvinova, P. Ring, and V. Tselyaev, Phys. Rev. C **75**, 064308 (2007).
[12] E. V. Litvinova and A. V. Afanasjev, Phys. Rev. C **84**, 014305 (2011).
[13] G. Colò, L. Cao, N. Van Giai, and L. Capelli, Comput. Phys. Commun. **184**, 142 (2016).
[14] J. Rowe, J. Math. Phys. **10**, 1774 (1969).
[15] B. A. Brown, Phys. Rev. C **58**, 220 (1998).
[16] E. Chabanat, P. Bonche, P. Haensel, J. Meyer, and R. Schaeffer, Nucl. Phys. A **643**, 441 (1998).
[17] D. Montanari *et al.*, Phys. Lett. B **697**, 288 (2011).
[18] D. Montanari, S. Leoni, D. Mengoni, J. J. Valiente-Dobon, G. Benzoni, N. Blasi, G. Bocchi, P. F. Bortignon, S. Bottoni, A. Bracco, F. Camera, P. Casati, G. Colo, A. Corsi, F. C. L. Crespi, B. Million, R. Nicolini, O. Wieland, D. Bazzacco, E. Farnea, G. Germogli, A. Gottardo, S. M. Lenzi, S. Lunardi, R. Menegazzo, G. Montagnoli, F. Recchia, F. Scarlassara, C. Ur, L. Corradi, G. deAngelis, E. Fioretto, D. R. Napoli, R. Orlandi, E. Sahin, A. M. Stefanini, R. P. Singh, A. Gadea, S. Szilner, M. Kmiecik, A. Maj, W. Meczynski, A. Dewald, T. Pissulla, and G. Pollarolo, Phys. Rev. C **85**, 044301 (2012).
[19] G. Bocchi *et al.*, Phys. Lett. B **760**, 273 (2016).
[20] I. Hamamoto, Nucl. Phys. A **126**, 545 (1969).
[21] P. F. Bortignon, R. A. Broglia, D. Bes, and R. Liotta, Phys. Rep. **30**, 305 (1977).
[22] D. A. Varshalovich, A. N. Moskalev, and V. N. Khersonskii, *Quantum Theory of Angular Momentum* (World Scientific, Singapore, 1988).
[23] J. Suhonen, *From Nucleons to Nuclei: Concepts of Microscopic Nuclear Theory* (Springer, Berlin, 2007).